8 An Ultraviolet Radiation Monitoring and Research Program for Agriculture

Wei Gao[1], John M. Davis[1], Roger Tree[1], James R. Slusser[1], and Daniel Schmoldt[2]

[1] United States Department of Agriculture UV-B Monitoring and Research Program
Natural Resource Ecology Laboratory
Colorado State University, Fort Collins, CO, USA
E-mail: wgao@uvb.nrel.colostate.edu
[2] United States Department of Agriculture
Cooperative State Research, Education, and Extension Service
Washington, DC, USA
E-mail: dschmoldt@csrees.usda.gov

Abstract The United States Department of Agriculture (USDA) Ultraviolet-B Monitoring and Research Program (UVMRP) was initiated in 1992 through a grant to Colorado State University (Fort Collins, CO, USA), authorized by Congress under the USDA Cooperative State Research Education and Extension Service (CSREES) Special Research Grant authority, to provide the agricultural science research community with the information necessary to determine if changing levels of UV-B radiation would threaten food and fiber production in the United States. The UVMRP consists of three major components: (1) monitoring solar radiation with an emphasis on UV-B radiation; (2) research to determine the effects of UV radiation on specific plants and crops; and (3) crop growth and production assessment modeling to assess the impact of climate change scenarios on crop production. The monitoring network, consisting of UV and visible solar radiation measurement instrumentation installed at 37 climatological sites, is described in this chapter, along with the basic algorithms used to process the data and the calibration methods designed to provide accurate long term data records. Procedures developed to provide aerosol optical depth, columnar ozone, and enhanced products, such as integrated irradiances weighted with biological spectral weighting functions and summed over selected time periods, are also described. An updated, flexible web page interface that allows users to access various data products is documented. The UVMRP's role in UV-B agricultural effects studies is summarized, including contributions by scientists at several collaborating

universities. The UVMRP's component that models agricultural sustainability by coupling a state of the science climate forecasting model to crop growth models in order to obtain the impact of climate change scenarios on crop yield is introduced. Future directions of UVMRP are also presented.

Keywords USDA UVMRP, ultraviolet, solar UV-B radiation, monitoring network, crop damage, UV climatology, agricultural sustainability, column ozone, crop yield

8.1 Introduction

Over the past few decades, the atmospheric science community has found it beneficial to establish routine programs to monitor various surface radiation quantities. During the early 1970s, a focus on the potential national benefit for using solar radiation as an energy source prompted the National Oceanic Atmospheric Association (NOAA) to begin monitoring solar radiation at its Climate Monitoring and Diagnostics Laboratory, currently known as the Earth System Research Laboratory (ESRL); see http://www.esrl.noaa.gov/gmd/publications/annrpt23/chapter3_2.htm. Although this initial interest in solar energy waned somewhat before its recent revival, the launch of the first meteorological satellites excited climate scientists by making estimates of the earth's radiation budget feasible from space. The first part of this effort started in the mid 1980s with the Earth Radiation Budget Experiment (ERBE), during which time surface monitoring of the radiation budget fields received renewed attention (Barkstrom, 1984). In the years that followed, as the need for more accurate estimates of the solar radiation budget for application in higher resolution climate models became desirable, and the concern over global climate change increased, the US Department of Energy funded the development of the Atmospheric Radiation Monitoring Program in 1989 (see http://www.arm.gov/about/). Satellite observations revealed another potential impact of anthropogenic activity during the 1980s, namely the observed depletion of stratospheric ozone in the Antarctic area (Farman et al., 1985; WMO, 1989; Stolarski et al., 1992) and the Arctic. These observations raised serious concerns in the scientific community of concomitant increases in ultraviolet-B (UV-B) radiation reaching the earth's surface (Frederick and Snell, 1988; Scotto et al., 1988; Grant, 1988; Worrest et al., 1989; Blumthaler and Ambach, 1990; Smith et al., 1992; Kerr and McElroy, 1993; Jaque et al., 1994; Herman et al., 1996) and its detrimental effects on plants, animals, ecosystems, and human health. These concerns led to the establishment of a network for monitoring solar radiation that was not concerned with the total solar and infrared spectrum, but rather specifically focused on the challenge of monitoring the UV radiation reaching the earth's surface, for evaluation of potential impact on crop yield and nutrition, and for assessing possible impacts on human and animal health (Caldwell et al., 1986;

Teramura et al., 1990). The purpose of this chapter is to document the activities associated with the monitoring of UV radiation, which has become one focus of the United States Department of Agriculture's UV-B Monitoring and Research Program.

8.2 Introduction to the USDA UVMRP (Purpose and History)

The beginnings of the USDA UVMRP stem from a series of USDA sponsored workshops, held for the purpose of determining the type of response that might be necessary to address the potential threat of UV radiation to US agriculture (Gibson 1991, 1992; Science and Policy Associates, 1992; O'Hara and O'Hara, 1993). Workshop participants, representing various universities, research institutions, and governmental agencies, recommended that the USDA establish a monitoring network to support research for determining the geographical distribution and temporal trends of the effects of UV-B radiation on plants and animals.

The USDA UVMRP was initiated in 1992, through a grant to Colorado State University (Fort Collins, CO, USA) authorized by Congress under the USDA Cooperative State Research Education and Extension Service (CSREES) Special Research Grant authority, to provide the agricultural science research community with the information necessary to determine if changing levels of UV-B radiation would threaten food and fiber production in the U.S. (Bigelow et al., 1998). The primary objective of the program was defined as providing information to the agricultural research community about the geographic and temporal distribution of UV-B irradiance in the U.S. It was recognized later, however, that there was a critical need for experimental and modeling research to examine the effects of enhanced UV-B radiation levels on crops and animals in order to meet the USDA objectives and to cope with the emerging challenges from the scientific community, such as the quantification of the effects, their variations among species and biochemical processes, their interactions with other biotic and abiotic factors, and gene control responses to UV-B radiation. Although some recent measurements indicate the start of a turnaround in stratospheric ozone, its recovery will likely take decades and is influenced by many factors (Staehelin et al., 2001; Newchurch et al., 2003; Reinsel et al., 2005; WMO, 2007). Great uncertainties exist in the future levels of surface UV radiation because it will be additionally affected by changes in clouds and aerosols (Bredahl et al., 2004; Kerr, 2005; McKenzie et al., 2007). The effects of UV radiation on plants, animals, ecosystems, and human health are complex and interact with other stress factors (Rozema et al., 1997; Yuan et al., 1998; Grant, 1999; Tegelberg et al., 2002; Gao et al., 2002, 2003; Caldwell et al., 2003; Clarke and Harris, 2003; Flint et al., 2003; Kulandaivelu and Tevini, 2003; Kakani et al., 2003; Reddy et al., 2003; Warren et al., 2003; Bassman, 2004; Turtola et al., 2005). Observations of visible and UV solar radiation reaching the

ground are necessary in order to quantify changes in atmospheric transmission which in turn drive the terrestrial ecosystems.

The UVMRP consists of three major components: (1) quality solar measurement and research in atmospheric radiation transfer, especially in UV wavelengths; (2) research to determine the effects of enhanced UV radiation on specific plants and agricultural crops to develop methods to lessen these effects and ensure crop productivity; (3) crop growth and production assessment modeling that accurately responds to various precipitation, temperature, and solar radiation scenarios. This chapter describes the UVMRP with an emphasis on the Program's data and derived products, the web-accessible database, and its role in facilitating research on agricultural effects, establishment of crop growth, and a production assessment modeling system.

8.3 Monitoring Network

8.3.1 Sites and Coverage

The design goal of the network was to have a 5° latitude × 10° longitude equal-area representation of the continental U.S. with additional coverage of Alaska and Hawaii (Bigelow et al., 1998). However, the existing distribution of the observation sites is not ideal because of logistical difficulties in securing acceptable sites in each latitudinal zone (Bigelow and Slusser, 2000). As of 2008, 34 climatological sites in the U.S., with 2 additional collaborating climatological sites in Canada and one in New Zealand, are operating in the network (Fig. 8.1). Sites were selected to represent each grid rectangle based upon their long-term viability, proximity to agricultural, biological, ecological, and ongoing UV research sites, unobstructed sky view, and availability of phone, internet, and power supply. The sites in Canada and New Zealand were set up for the purpose of maintaining a scale for comparison of each country's radiation archives. In addition, ad hoc research sites are temporarily set up and maintained for specific research purposes for a period of time. Six high resolution U1000 spectroradiometers were sited at research sites where key collaborative research allowed interdisciplinary uses of the data, although the high maintenance of the U1000s eventually led to discontinuing their deployment. Instruments at a research site may be turned off and on at any time, and additional instruments can be installed and run for a period of time depending on the purpose of the research project, especially during the campaigns of inter-comparisons between instruments from different manufacturers. On the other hand, the climatological sites require less sophisticated instrumentation than at research sites, and the instruments at a climatological site operate continuously without intentional interrupts except for routine maintenance. In this chapter, we focus on the climatological sites only.

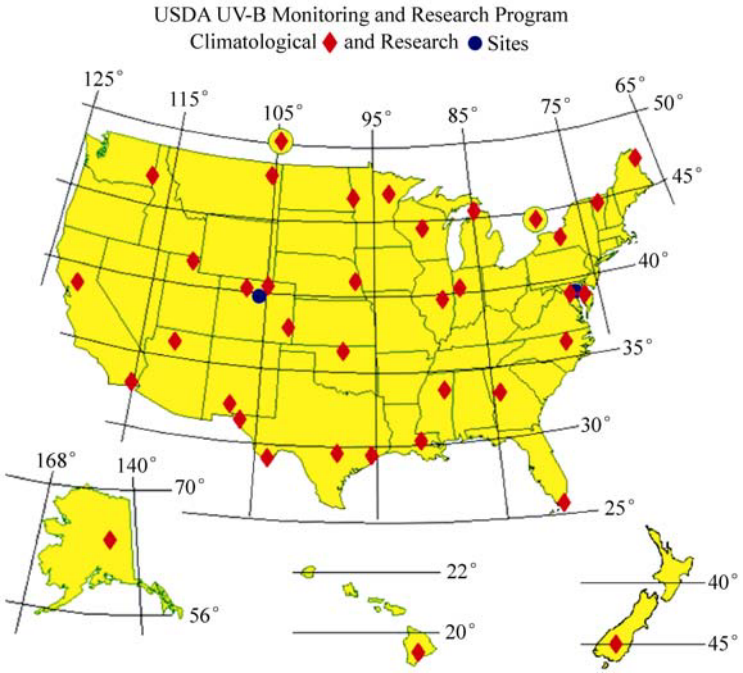

Figure 8.1 The UVMRP monitoring network coverage from 1993 through year-end 2008

8.3.2 Data Products Provided by UVMRP

The USDA UVMRP provides a wide variety of products to the broader scientific community. Although the primary stakeholders of UVMRP are focused on agricultural applications, many users of the data access the products via the web page or by special request for use in human health research, atmospheric science studies, industrial coating testing and analysis, defense contractor work, and for a few proprietary applications.

The data provided by UVMRP may be divided into measurement data and derived products. Many quantities are measured and the values are available on the UVMRP web site within 24 hours (http://uvb.nrel.colostate.edu). This also applies to some of the derived products. Table 8.1 presents a list of quantities categorized as either direct measurements or derived quantities, along with the instrument used to collect the data. Section 8.4 elaborates on the data collection process in general, and the processing applied to arrive at useful quantities. Section 8.5 follows with a discussion of the processing of the derived data products.

Table 8.1 The primary measurements and derived quantities available to users of the USDA UVMRP website. Other related quantities are available upon request

Data Product	Brief Description	Primary or Derived	Instrument Name
UV spectral irradiance	300, 305, 311, 317, 325, 332 and 368 nm wavelengths	Primary	YES* Inc. UV-MFRSR
UV erythemal irradiance	280 nm − 320 nm (erythemally weighted)	Primary	YES Inc. UVB-1 pyranometer
Visible spectral irradiance	415, 500, 615, 673, 870, and 940 nm wavelengths	Primary	YES Inc. VIS-MFRSR
PAR	400 nm − 700 nm Photosynthetically Active Radiation	Primary	LI-COR** Inc. LI-190SA Quantum Sensor
Surface reflected irradiance	Used to indicate presence of snow covered surface	Primary	LI-COR Inc. LI-210SA photometer
UVA broadband irradiance	320 nm − 400 nm broadband irradiance (at only 7 sites)	Primary	Solar Light*** Model 501A -UV-A radiometer
Ambient air temperature and relative humidity	Standard meteorological values	Primary	Vaisala**** HMP 35A or HMP 45D
Ambient barometric pressure	Standard meteorological values (at only 14 sites)	Primary	Vaisala Inc. Model PTB-101 or PTB-110
Aerosol optical depth	332 nm and 368 nm instantaneous or daily averaged	Derived from MFRSR	
Column ozone	Daily value	Derived from UV-MFRSR	
Synthetic spectrum	300 nm − 400 nm irradiance at 1 nm resolution	Derived from UV-MFRSR	
UV climatology	UV-A, UV-B, Erythemal, Flint, Caldwell, Vitamin D as daily, monthly, and annual sums	Derived from synthetic spectrum	

* Yankee Environmental Systems, Turners Falls, MA
** LI-COR Biosciences, Lincoln, NE
*** Solar Light, Glenside, PA
**** Vaisala Inc., Vantaa, Finland

8.4 Data Collection and Processing

Two data loggers are installed at each site to collect and transfer the direct measurements from the instruments referred to in Table 8.1. One data logger is used to collect the data every 15 seconds from the VIS-MFRSR, UVB-1 pyranometer, temperature/humidity sensors, and the downward looking LI-COR 210SA photometer. The other is for the UV-MFRSR, PAR Quantum sensor, and barometer (and UV-A radiometer where applicable) that are sampled every 20 seconds. The difference between the sampling frequencies results from a longer required dwell time of the UV-MFRSR instrument. The data are aggregated into 3-min averages and stored in each data logger. Figure 8.2 shows an example of a UVMRP station.

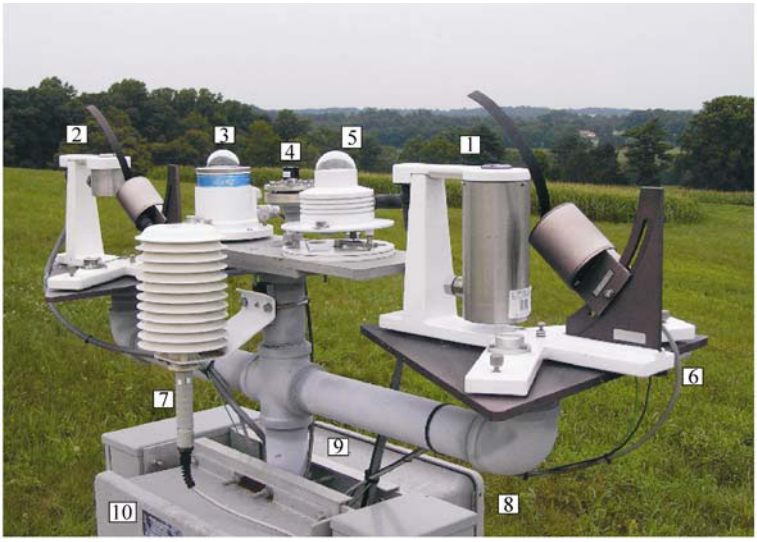

Figure 8.2 The layout of instruments at a typical climatological site in the UVMRP monitoring network. (1) UV-B Multi-Filter Rotating Shadowband Radiometer (UV-MFRSR); (2) Visible Multi-Filter Rotating Shadowband Radiometer (vis-MFRSR); (3) UVB-1 Pyranometer (erythemal); (4) Photosynthetically Active Radiation (PAR or Quantum Sensor); (5) UV-A biometer (only at 7 sites); (6) Downward-looking photometer; (7) Air temperature and relative humidity sensor; (8) Barometric pressure (14 sites, inside datalogger enclosure); (9) UV-MFRSR Datalogger; (10) Vis-MFRSR Datalogger

The instruments are located at sites with unobstructed horizons and are positioned at a level of 1.5 m above the ground. The temperature and relative humidity measurements are intended to be used in applications that require these data to be collocated with the radiation measurements and are not intended as substitutes for the National Weather Service (NWS) data, since these sensors are not installed in conformance to NWS standards. The data loggers are driven by AC power with rechargeable batteries in line to act as a backup in case the AC power fluctuates or outages occur for a short period of time. The "raw voltage" measurements from the station data loggers are transferred to the UVMRP data server every day through dedicated phone lines or the Internet. The raw voltages are processed into their corresponding physical quantities at the UVMRP headquarters located at Colorado State University, Fort Collins, CO, USA. Data quality control measures are applied daily. Discussion in this section will focus on the UV-B data, including UV-MFRSR and UVB-1 measurements.

Before 1997, characterization and calibration of the UV-MFRSR, VIS-MFRSR, and UVB-1 instruments were done annually at YES or at the Atmospheric Science Research Center (ASRC) at the State University of New York (SUNY)-Albany, NY, USA. Since 1997, annual characterization and calibration of the UV-MFRSR and UVB-1 instruments have been performed at the Central UV Calibration Facility

(CUCF), which is housed within NOAA's ESRL. The CUCF was initiated and developed in collaboration with the Optical Technology Division of the National Institute of Standards and Technology (NIST) and works to transfer the NIST standards of spectral irradiance to the U.S. solar UV radiation monitoring community in an accurate, long-term, repeatable, and cost-efficient manner (Disterhoft, 2005). The characterization and calibration of VIS-MFRSR instruments are based on the original YES values. Because many of the VIS-MFRSR instruments have been deployed for many years, the users are warned of this on the UVMRP website and are encouraged to use Langley calibrations, which are updated monthly. Until recently, the UV-MFRSRs were cycled through the calibration process at CUCF on an annual basis. Beginning in 2006, program priorities and fiscal constraints significantly lengthened the period between laboratory calibrations. Until this situation is resolved, the users of these data may wish to consult the most recent deployment date listed for the instrument at the site of interest via the UVMRP web page under "Site Location Deployment History", to check for last lamp calibration date. Then the choice of using lamp or Langley calibrations for spectral UV data may be made. The PAR sensors are sent to LI-COR for recalibration at their recommended two-year interval. The rest of the instruments, LI-COR 210SA photometers, and temperature-humidity probes, are calibrated by the manufacturers before they are deployed.

8.4.1 UV-MFRSR Data Processing

The UV-MFRSR uses independent interference filter-photodiode detectors and an automated rotating shadow band to measure the total horizontal and diffuse horizontal UV solar irradiance at seven wavelengths concurrently (Michalsky et al., 1988; Harrison et al., 1994). Direct normal irradiance is determined within the data logger by subtracting the diffuse from the total signal, followed by a correction for imperfect cosine response. The UV-MFRSR instruments provide synchronized measurements of spectral irradiances within the UV wavelength region. The direct normal measurement provides an input required for retrieval of atmospheric optical properties, including air mass components, such as the aerosol optical depths and columnar ozone content that may not be feasible from the total irradiance signal alone. Essential adjustments to the UV-MFRSR measurements include removal of dark current bias voltages and a correction for deviations of the sensors from an ideal cosine response. The corrected voltages are then converted into irradiances by multiplying by a calibration factor.

8.4.1.1 Dark Current Bias Removal

Certain extraneous voltages may be generated by the electronics of the observation system, including data loggers, amplifiers, circuits, and connecting wires. These

signals are measured at night in the absence of solar radiation using voltages averaged from one hour prior to, and one hour after, the time of minimum solar elevation over the three day period preceding the current data processing day. For a more detailed discussion of the dark current voltage bias removal, please view the USDA UVMRP website (http://uvb.nrel.colostate.edu/UVB/index.jsf), under the "Monitoring Network," then the "Data Processing Procedures" links.

8.4.1.2 Cosine Correction

The direct beam irradiance measured on a horizontal surface is given by the product of the incident normal irradiance and the cosine of the solar zenith angle (SZA). However, the detectors of the UV-MFRSR do not have perfect cosine responses, especially at higher incidence angles. The correction for the deviation of the response from an ideal cosine response is known as cosine correction or angular correction. The non Lambertian response of the UV-MFRSR instruments has been described by Harrison et al. (1994). Characteristics of the cosine responses of the UV-MFRSR instruments used in the network are described by Bigelow et al. (1998). The actual angular responses of an instrument are a function of solar zenith and azimuth angles and were determined annually by YES (in the initial periods of network operation and by CUCF since 1997). The cosine response is determined through laboratory measurements based on an independent radiometric characterization of individual detectors made through the diffuser along two orthogonal planes (Michalsky et al., 1995). With knowledge of angular responses along north-south and east-west azimuths, correction factors for direct normal voltages are interpolated according to solar zenith and azimuth angles at the time of measurement.

An imperfect cosine response affects the measurement of the diffuse horizontal irradiance in addition to the direct normal component (Leszczynski et al., 1998). Experimental results show that the uncertainties in diffuse irradiance due to the assumption of a homogeneous sky radiance distribution are within ±1.5% in the UV-B band for varying atmospheric and geographic conditions (Gröbner et al., 1996). This assumption is employed in processing the diffuse irradiance values of the UV-MFRSR.

8.4.1.3 Out-of-Band Correction

In the original design of the UV-MFRSR the two channels at 300 nm and 305 nm used silicon-carbide (SiC) photodiodes and the remaining five channels used gallium-phosphide (GaP) photodiodes. By the end of 1997, this instrument design had been deployed at the 22 sites, which comprised the climatological network at that time. In December of 1997, the first of many failures of GaP photodiodes occurred ultimately resulting in a solution developed jointly by UVMRP and YES which involved the replacment of the GaP photodiodes with silicon (Si) versions. The GaP photodiodes were replaced with silicon in all UVMRP UV-MFRSRs by

the end of 2002. Thus, the UV-MFRSRs now use Si photodiodes in the 311 nm through 368 nm channels and retain the original SiC photodiodes for the two channels centered at 300 nm and 305 nm (Janson et al., 2004).

Ideally, a radiometer should be designed to reject all radiation outside the designated wavelength region, i.e., in the 2 nm wide wavelength band of each of the seven channels. However, laboratory tests showed that the replacement Si photodiodes allowed out-of-band light from the NIST traceable tungsten-halogen lamps during the calibration procedure to contribute to the calibration signal, resulting in an inaccurate calibration (Lantz et al., 2005). Further studies revealed that the contribution of out-of-band light to the signal depended on several factors, including the channel, the individual instrument, and the lamp used for the laboratory calibration. Further analysis revealed that the out-of-band light contributing to the signal is mainly from wavelengths longer than 570 nm. This contribution of out-of-band light is commonly referred as "red light leakage" or "red leakage" for simplicity. To characterize the contribution of out-of-band light to the signal, each of the UV-MFRSR instruments were measured for out-of-band rejection using short-pass cutoff filters in the field with the sun as the radiation source and in the laboratory using the lamp as the radiation source. Results are given in Tables 8.2 and 8.3. Forty-seven UV-MFRSR instruments were tested in the field for out-of-band light and showed negligible signal within the detection limit of the measurements when the sun is used as the radiation source (Table 8.2). The largest average percent contribution is in the 317 nm channel. The average contribution of out-band-light is 0.4% of the total solar signal, with a maximum of 1.3% for this channel. The implications are that the Langley plot calibrations, which are described below, are not affected by red light leakage to any significant extent. All UV-MFRSR instruments were tested in the laboratory for out-of-band light using a FEL-type quartz-tungsten-halogen lamp as the radiation source and a 400 nm long pass filter. As shown in Table 8.3, there is a significant percentage of out-of-band light contributing to the signal when a lamp is used as the calibration source. The most significant contribution from the out-of-band light is in the 317 nm channel where the average is 22.1%. All of the channels with Si photodiodes have a detectable out-of-band contribution to the total lamp signal. The two channels using SiC photodiodes have no measurable out-of-band signal.

Table 8.2 Percent contributions of out-of-band light to the measured solar signal from 47 filter radiometers (from Lantz et al., 2005)

	300 nm	305 nm	311 nm	317 nm	325 nm	332 nm	368 nm
Average	0.1%	0.0%	0.2%	0.4%	0.1%	0.1%	0.1%
Maximum	0.0%	0.3%	0.5%	1.3%	0.3%	0.4%	0.5%
Minimum	0.0%	0.0%	0.0%	0.0%	0.0%	0.0%	0.0%

Table 8.3 Percent contributions of out-of-band light to the measured lamp signal during calibration with a FEL-type quartz-tungsten-halogen lamp from 40 filter radiometers (from Lantz et al., 2005)

	300 nm	305 nm	311 nm	317 nm	325 nm	332 nm	368 nm
Average	0.0%	0.0%	8.8%	22.1%	12.1%	11.2%	4.0%
Maximum	0.1%	0.1%	28.4%	35.7%	28.5%	23.1%	10.5%
Minimum	0.0%	0.0%	4.2%	6.6%	3.9%	4.9%	1.1%

The calibration factors corrected for out-of-band signals for the Si photodiodes are applied to the corrected voltages (after the dark current voltage bias and cosine correction) to convert them into irradiances, which are the lamp calibrated channel data provided to the public through an internet website. Earlier versions of the UV-MFRSR instruments that used the GaP photodiodes participated in several North American Interagency Inter-comparisons of Ultraviolet Spectroradiometers conducted during 1995 – 1997. The measurements of the UV-MFRSR instruments agreed with the filter-weighted irradiances of the participating spectroradiometers with a ±5% uncertainty at local noon (Early et al., 1998a, 1998b; Lantz et al., 2002). Collocated measurements show that after the out-of-band corrections are applied, the irradiances measured by a representative UV-MFRSR instrument using Si photodiodes agree with the filter-weighted irradiance measurements from a U1000 spectroradiometer within the uncertainty of ±1.5% (Lantz et al, 2005) for the seven channels. All lamp calibrated UV-MFRSR data accessed via the UVMRP website has now been corrected for the out-of-band radiation leakage.

8.4.2 Erythemally Weighted UV Irradiance

One of the data types most frequently requested from UVMRP is a compilation of erythemally weighted irradiance over a specified geographic region and time period. The UVMRP employs YES UVB-1 pyranometers to measure the Commission Internationale de l'Eclairage (CIE) weighted erythemal irradiances (McKinlay and Diffey, 1987) at each climatological site. Initially, the UVB-1 pyranometers were calibrated and characterized annually by the instrument manufacturer. Comparisons between collocated radiometers show an agreement of better than ±2.3% when SZA is less than 80°, while absolute errors might reach 10% when SZA is greater than 80° (Bigelow et al., 1998; McKenzie et al., 2006). Since 1997, the broadband pyranometers have been calibrated and characterized annually by CUCF. Characterizations include the tests of cosine response and spectral response. The scale factor for erythemal calibration is determined by matching the output of the pyranometer to the standard triad at CUCF. The absolute calibration factor of the broadband pyranometer is determined annually by comparing the output of the broadband sensor in sunlight with that of three collocated UVB-1 standard

pyranometers (triad). The inter-comparison with the triad typically lasts from one to two months in order to obtain sufficient data for the calibration that includes corrections for different amounts of columnar ozone in each zenith angle regime. The standard triad is in turn frequently calibrated for erythemal action spectrum as a function of SZA and total column ozone in the field against a collocated precision spectral radiometer employing the principle described in the literature (Grainger et al., 1993; Lantz et al., 1999; Xu and Huang, 2000; Vijayaraghavan and Goswami, 2002; Xu and Huang, 2003). This practical calibration scheme is supported by the uniformity of the cosine responses of different broadband pyranometers in the UVMRP network. The uncertainty in this calibration is from two sources. One consists of the random and systematic uncertainties of the ozone and SZA dependent erythemal calibration factor. The other is the difference in the scale factor for each pyranometer.

Although the absolute calibration uncertainty of the pyranometers could reach as high as ±10%, relative uncertainties among the pyranometers are more important in certain applications (McKenzie et al., 2006). Differences in spectral response and angular response are the major sources for relative uncertainties. These differences are inherent in the calibration procedure, which is a comparison of the solar signal from the pyranometer to the triad as measured at CUCF. In order to examine the relative accuracy of the instruments, experiments that compared the solar signal from the standard triad to the field site UVB-1 pyranometers were conducted as the instruments cycled through the calibration process. The tests were performed as a function of SZA over 110 two-week periods under various weather conditions. The results indicate the rather remarkable level of consistency amongst the pyranometers in that, on average, the pyranometers differ from the standard triad by 0.1% at an SZA of 20°, and by 2.8% at an SZA of 80° for all 51 tested instruments. Other collocated measurements of the UVB-1 pyranometers also show a good agreement with the broadband pyranometers from other manufacturers, as well as within the tested UVB-1 pyranometers (Seckmeyer et al., 2007). Since a generic factor is applied for ozone-dependent calibration, differences of spectral responses between the pyranometers may introduce uncertainties. In order to more fully characterize the individual pyranometers, their signals are corrected for cosine response, and for the purposes of determining erythemal irradiance, individual characterizations as a function of zenith angle and total column ozone are made as discussed below.

8.4.2.1 Angular (Cosine) Response of the UVB-1 Pyranometer

The erythemal irradiance is almost always supplied as a total horizontal quantity. Thus, the angular response of each UVB-1 instrument must be utilized to correct for imperfect cosine response. The angular response is tested annually by performing a north-south scan and an east-west scan with an interval of one degree zenith angle. The average of the two scans is considered as the cosine response. Figure 8.3 displays the relative angular responses of 10 UVB-1 pyranometers that were

characterized by the CUCF in 2004. The measurements are normalized to 0° SZA. These results have the typical shapes of those reported by previous studies (Grainger et al., 1993; Mayer and Seckmeyer, 1996; Landelius and Josefsson, 2000). The differences of the angular responses from an ideal cosine response have been discussed by Bigelow et al. (1998). Although the departure from the ideal cosine response exceeds 10% beyond 60° SZAs (Bigelow et al., 1998), the variability between different pyranometers is rather small. Figure 8.3 actually displays the cosine response of ten instruments and shows that the agreement is within the width of the plotted line. Figure 8.4 shows the standard deviations of the cosine responses of 20 randomly selected pyranometers. The variances tend to increase with SZA, but the standard deviations are within 0.02% in the zenith angle range of 0° – 89°. This repeatability among the angular responses of the UVMRP broadband pyranometers suggests that a single generic cosine correction may be applied to all pyranometers in the network without introducing significant uncertainties.

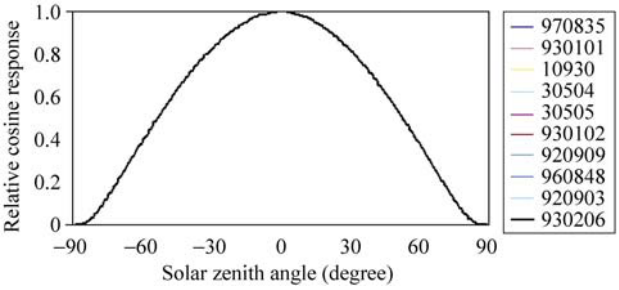

Figure 8.3 Normalized cosine responses of ten UVB-1 pyranometers. Numbers in the legend indicate the serial numbers of the sensors. The 10 curves are overlaid over each other. It is difficult to visibly separate them, which exhibits uniform cosine responses

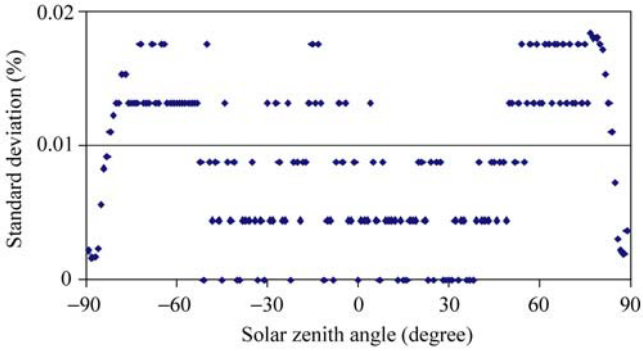

Figure 8.4 Standard deviations of cosine responses of 20 UVB-1 pyranometers as a function of SZA. The results show that the responses are within 0.02% of the mean cosine response and generally within the digitization error of the data logger

8.4.2.2 UVB-1 Spectral Response and Influence of Columnar Ozone

The erythemally weighted irradiance is determined by convolving the CIE action spectrum (McKinlay and Diffey, 1987) shown in Fig. 8.5 with the measured spectral irradiance. Measuring the erythemal UV irradiances requires that the spectral response of the pyranometer is identical with the CIE action spectrum because the spectral distribution of the solar radiation varies with many factors, such as ozone content, SZA, clouds, and other components in the atmosphere. However, the spectral response of the UVB-1 broadband pyranometer does not perfectly simulate the CIE action spectrum (Fig. 8.5), especially in the regions of shorter and longer wavelengths. Therefore, all factors that affect the wavelength distribution of solar irradiance in the erythemal wavelength band will impose potential impacts on the measurements of erythemal UV irradiance. The most significant variables are SZA, total ozone content and aerosol optical properties (Bodhaine et al., 1998; Lantz et al., 1999). Considering the effects of ozone content and SZA, the erythemal calibration factors for the UVB-1 broadband pyranometers are determined by the CUCF as a function of SZA and total ozone, or as a function of SZA with the assumption that the overhead total column ozone is 300 DU. The latter calibration factors are more conveniently applied when ozone measurements are not available at a site. The UVMRP data set provides erythemal UV irradiance data with the calibration factors of SZA dependence that assume overhead column ozone is 300 DU. Due to variable ozone contents and SZA, this assumption may result in an error of up to 25% (Fig. 8.6) for the ozone range of 200 DU − 500 DU for different SZAs. For a more accurate erythemal irradiance data set, however, ozone correction will be necessary. Lantz et al. (1999) detailed

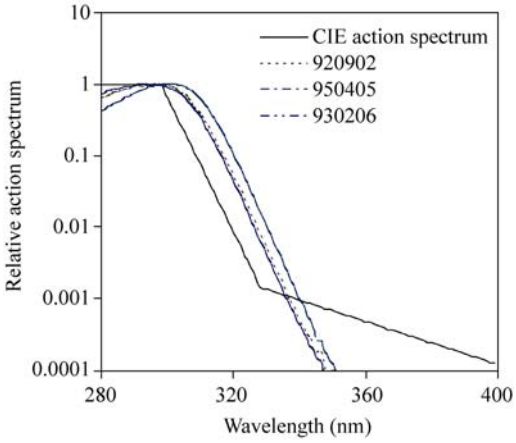

Figure 8.5 CIE action spectrum and spectral responses of three UVB-1 pyranometers. The numbers in the legend indicate the serial numbers of the tested sensors

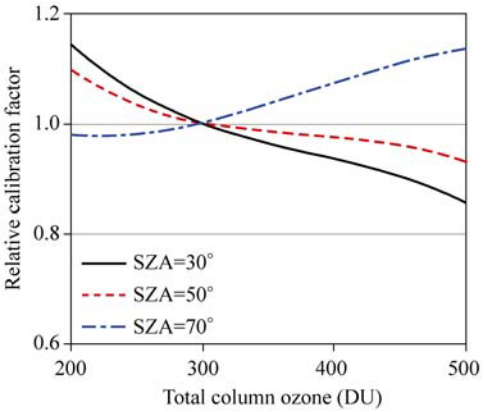

Figure 8.6 Erythemal calibration factors for the UVB-1 as a function of total column ozone for three SZAs normalized by their respective values for total column ozone of 300 DU

an approach to derive erythemal UV irradiance on clear days. This method is also recommended by the World Meteorological Organization/Global Atmosphere Watch (Seckmeyer et al., 2007) for erythemal calibration of broadband pyranometers. In the proposed scheme, the dependence of the calibration factor on ozone is curve-fitted with a third order polynomial for different SZAs from 5° to 80° using a step interval of 5°. Factors between the step intervals can be interpolated using any efficient interpolating technique. In cases where the total column ozone is known to differ significantly from 300 DU, the user may contact UVMRP to obtain erythemally weighted irradiances calibrated at other ozone levels.

8.4.3 Langley Analysis

While the laboratory calibrations and characterizations of the UV-MFRSR instruments were routinely performed, an alternative technique that has been used for many decades in various applications is the Langley plot method (Shaw, 1982; Thomason et al., 1983; Wilson and Forgan, 1995; Slusser et al., 2000). The Langley plot is used to provide more frequent calibrations of both the UV and VIS MFRSRs. The Langley method is based on the Beer-Lambert law, which describes the attenuation of the sun's direct-beam monochromatic radiation passing through the earth's atmosphere and is expressed mathematically (Thomason et al., 1983; Wilson and Forgan, 1995) as:

$$I_\lambda = R^2 I_{0,\lambda} \exp\left(-\sum \tau_{\lambda,i} m_i\right) \tag{8.1}$$

In Eq. (8.1), I_λ is the direct normal irradiance at the ground at wavelength λ, R^2

denotes a correction for the earth-sun distance at the time of measurement, $I_{0,\lambda}$ represents the extraterrestrial irradiance, $\tau_{\lambda,i}$ is the optical depth for the *i*-th air component, and m_i stands for the air mass of the *i*-th air component through the atmosphere. Taking the natural logarithm of both sides, we have

$$\ln I_\lambda = \ln\left(R^2 I_{0,\lambda}\right) - \sum \tau_{\lambda,i} m_i \,. \tag{8.2}$$

Provided that the irradiance is obtained by applying a calibration factor to the voltage output of the radiometer, the Beer-Lambert law can also be applied to the voltage of the instrument measurement. For the raw voltage output of the detector the formula is:

$$\ln V_\lambda = \ln\left(R^2 V_{0,\lambda}\right) - \sum \tau_{\lambda,i} m_i \,. \tag{8.3}$$

In Eq. (8.3), V_λ is the measured voltage at wavelength λ, and $V_{0,\lambda}$ represents the voltage the detector could measure oriented normal to the sun at wavelength λ outside the earth's atmosphere at one Astronomical Unit. Assuming that the optical depth remains constant over a period of time when the air mass, which is a function of SZA, changes significantly, the Langley analysis method determines the $V_{0,\lambda}$ by extrapolating voltage intercept at zero air mass when a linear fit to the logarithm of the measured voltage versus air mass is performed. Since the values of R and $I_{0,\lambda}$ can be accurately estimated (Lean 1991; Lean et al., 1997), a calibration factor (c_λ) to convert the measured voltage at wavelength λ into irradiance can be determined as:

$$c_\lambda = \frac{I_{0,\lambda}}{V_{0,\lambda}} \,. \tag{8.4}$$

The calibrated irradiance, $I_{\lambda,F}$, over the filter pass-band is obtained by multiplying the detector voltage measured at the ground by the calibration factor $c_{\lambda,F}$ (Bigelow et al., 1998). The calibration factor is determined using the filter-weighted integrations of $I_{0,\lambda}$ and $V_{0,\lambda}$ as follows (Slusser et al., 2000):

$$c_{\lambda,F} = \frac{\int I_{0,\lambda} F_\lambda \mathrm{d}\lambda}{V_{0,\lambda} \int F_\lambda \mathrm{d}\lambda}, \tag{8.5}$$

where F_λ is the filter function or spectral response function of the filter. After the direct and diffuse components of the voltage have been corrected for an ideal cosine angular response, the Langley analysis based on the objective algorithms (Harrison and Michalsky, 1994) is performed to determine $V_{0,\lambda}$. Obtaining the correct V_0 is essential in calibration. The V_0 values are generated for morning

and afternoons that supply at least 12 clear-sky measurements to the algorithm. The V_0 values are collected over air mass ranges that depend on the wavelength of the channel. For example, for the 300 nm through the 325 nm channels, the measurements for the direct beam voltages for an air mass range of 1.2 to 2.2 are used, while for the 337 nm and 368 nm channels, an air mass range between 1.5 and 3.0 is used. All the morning V_0 values deemed to be measured under clear sky for a given instrument at a given site are used as the ordinate in a linear regression routine using the air mass as the abscissa. The V_0 for the day is the offset derived from the regression routine.

Comparisons from previous studies of sun photometer calibration using the Langley analysis and the standard lamp in (Schmid and Wehrli, 1995; Schmid et al., 1998; Janson et al., 2004) show that the Langley analysis calibration is superior to the lamp calibration when the analysis is performed under very clear atmospheric conditions. However, the Langley calibration introduces more uncertainties at shorter wavelengths (around 300 nm) because the signals are weak. The Langley method cannot be applied in conditions where the Beer-Lambert law is not applicable such as over broad spectral bandpasses, or where multiple scattering may introduce path radiance into the detector's field of view. Other limitations of the Langley calibration method are discussed in Wilson and Forgan (1995), and Schmid et al. (1998). The combination of both types of calibration serve as an additional means of quality control; long term drifts from lamp calibrations can be detected by comparison with the Langley values whereas unresolved cloudiness in the Langley calibration data may be signaled by comparison with the lamp values. Thus, the use of a combination of both Langley calibration and lamp calibration is recommended to maintain a long term accurate calibration (Schmid and Wehrli, 1995). Figure 8.7 shows the results of the Langley analysis for two UV-MFRSR instruments deployed at Mauna Loa, HI. In the upper plot, 300 nm V_0s are shown, which are characteristically noisy due to a relatively low signal level as compared to the 305 nm channel data displayed in the lower plot.

8.4.4 Data Processing for Other Measurements

The VIS-MFRSR measurements are processed with the same procedures as for UV-MFRSR data with the exception noted above concerning the reliance on Langley calibrations since no recent lamp calibrations are available for the VIS-MFRSR. No out-of-band signals have been detected from the VIS-MFRSR instruments. For the PAR sensors, barometers, and temperature-humidity probes, calibration factors provided by the manufacturers are applied to the raw voltages to derive the final data products.

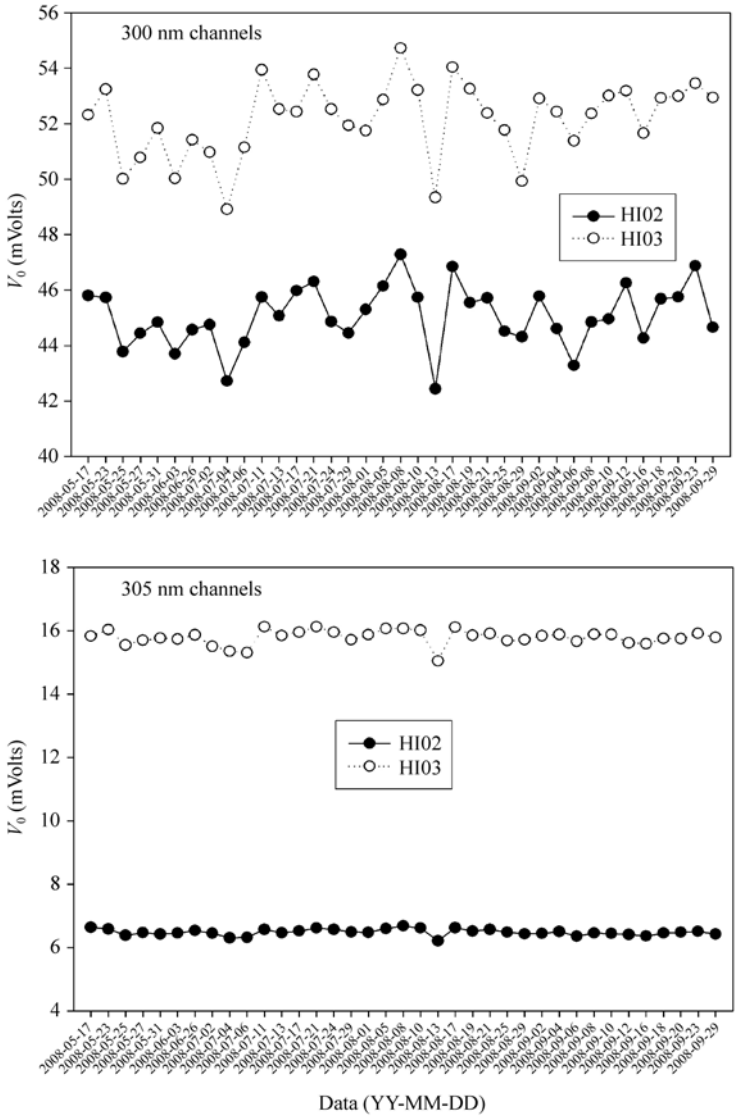

Figure 8.7 Plots of V_0 values from instruments HI02 (climatological site) and HI03 (research site) at Mauna Loa, HI derived from the Langley analysis method for the 300 nm and 305 nm channels from May 17 through September 29, 2008

8.5 Derived Products

By applying the techniques and algorithms developed in recent years to the measurements, various useful products can be derived. Examples of the derived products included in our database are optical depth, daily column ozone, and UV-B

irradiance with 1 nm spectral resolution. Using the synthetic spectrum algorithm discussed below, various agriculturally significant indices are derived, such as the Caldwell and Flint biologically weighted irradiances. An estimate of the vitamin D dosage is available, along with erythemally weighted irradiance and the closely related UV index. In addition to these products routinely available on the UVMRP website, numerous products are processed on demand for users in the agricultural, medical, and industrial materials communities.

8.5.1 Optical Depth

Optical depths are regularly acquired using measured spectral irradiances. These measurements are useful in developing regional aerosol climatology, validating satellite aerosol observations, and offering atmospheric corrections for satellite retrievals. Aerosol optical depth may also serve as a good indicator of surface visibility (Hand et al., 2004).

8.5.1.1 Instantaneous Optical Depth

Total and aerosol plus cloud optical depths are retrieved at 3-min intervals from the measurements of spectral irradiance. The total optical depths are derived using the Beer-Lambert law,

$$\tau_\lambda = \frac{\ln V_{0,\lambda} - \ln V_\lambda}{m}, \tag{8.6}$$

where τ_λ is the total optical depth and m denotes the air mass, which is a function of SZA. V_λ is the measured raw voltage value from the channel centered at wavelength λ. The value of $V_{0,\lambda}$ for each channel and the requested date are determined from a time series of Langley-generated voltage intercepts for morning periods of that day as discussed above. The Langley analysis is performed based on the objective algorithms developed by Harrison and Michalsky (1994), as discussed in Section 8.4.3.

For clear sky data, Rayleigh and ozone optical depths are subtracted from total optical depths to obtain the aerosol optical depths. Methods to accurately estimate Rayleigh optical depths in the atmosphere have been well documented in Fröhlich and Shaw (1980), Young (1981), Teillet (1990), Bucholtz (1995), and Bodhaine et al. (1999). We use the following formula to compute the Rayleigh optical depth for simplicity (Marggraf and Griggs, 1969; Stephens, 1994):

$$\tau_{\mathrm{Ray},z,\lambda} = 0.0088\lambda^{(-4.15+0.2\lambda)}\mathrm{e}^{\left(-0.1188z-0.00116z^2\right)}, \tag{8.7}$$

where $\tau_{\mathrm{Ray},z,\lambda}$ represents the Rayleigh optical depth at the altitude z (in km) and the wavelength is in the units of microns (μm). This formula is valid under the

assumption that the variation of air density with altitude follows the variation of pressure with altitude (Stephens, 1994).

Ozone optical depth is calculated by:

$$\tau_{O_3,\lambda} = \Omega \alpha_{O_3} c_{O_3} \tag{8.8}$$

where Ω is total column ozone in Dobson units, α_{O_3} is the ozone cross section, and $c_{O_3} = 0.001$ is a conversion constant. For UV wavelengths, the effective ozone cross sections are used (Bigelow et al., 1998). For visible wavelengths, the ozone absorption coefficients of Shettle and Anderson (1995) are used. Aerosol optical depth for clear days at 3-min intervals is then calculated by subtracting the Rayleigh optical depth and ozone optical depth from the total optical depth. These calculations are included in the UVMRP database. Note that aerosol optical depths are not available on cloudy days.

8.5.1.2 Average Optical Depth

The averaged optical depths for the mornings and/or afternoons are calculated from the instantaneous results. To ensure the accuracy of the results, time periods included in the averaging process are limited to specific air mass ranges which vary by wavelength: 1.5 – 3.0 for 332 nm and 368 nm, and 2.0 – 6.0 for 415 nm – 860 nm.

8.5.2 Daily Column Ozone

The algorithm for calculating the column ozone of the atmosphere is based on the work of Gao et al. (2001), which uses the direct-beam irradiance for the retrieval. Given spectral measurements of UV-B, the total column ozone Ω in Dobson units is calculated as:

$$\Omega = \frac{N_1 - N_2 - \left[\left(\beta_{305} - \beta_{325}\right) - \left(\beta_{311} - \beta_{332}\right)\right] m_a \left(P/P_0\right)}{\left[\left(\alpha_{305} - \alpha_{325}\right) - \left(\alpha_{311} - \alpha_{332}\right)\right] \mu} \times 10^3, \tag{8.9}$$

where

$$\begin{aligned} N_1 &= \ln \frac{V_{0,305}}{V_{0,325}} - \ln \frac{V_{305}}{V_{325}}, \\ N_2 &= \ln \frac{V_{0,311}}{V_{0,332}} - \ln \frac{V_{311}}{V_{332}}, \\ \mu &= \frac{R + h}{\left[\left(R + h\right)^2 - \left(R + z\right)^2 \sin^2 \theta\right]^{1/2}}, \end{aligned} \tag{8.10}$$

where the notations are:

β_λ Rayleigh scattering optical depth at wavelength λ;

m_a air mass corresponding to the SZA (θ) at the time when the measurement is taken;

P observed station atmospheric pressure;

P_0 mean sea level atmospheric pressure;

α_λ ozone absorption coefficient (base e) at wavelength λ;

$V_{0,\lambda}$ extraterrestrial voltage intercept at zero air mass at wavelength λ;

V_λ direct normal voltage after cosine and dark current bias corrections at wavelength λ;

μ ratio of the actual and the vertical paths of solar radiation through the ozone layer;

R average earth radius (6,371.229 km);

z height of the station above mean sea level;

h height of ozone layer above mean sea level at station location (20 km is assumed);

θ solar zenith angle.

Total column ozone is computed using those 3-min average measurements when the irradiance at 311 nm is greater than 0.002,5 $Wm^{-2}nm^{-1}$ and the condition $\theta > 70^\circ$ holds. Daily total column ozone is then determined by averaging these 3-min results if there are at least five of such 3-min averages.

8.5.3 Synthetic Spectrum Data

The UV-MFRSR instrument, described in Section 8.2.2, makes measurements every three minutes in seven spectral regions, each with a nominal bandwidth of 2 nm. The centers of the bandwidth regions are located at 300, 305, 311, 317, 325, 332 and 368 nm. The measurements are useful in assessing damage to plants and human health, particularly when considered in conjunction with specific Biological Spectral Weighting Functions (BSWFs); see for example Caldwell et al. (1986). The calculation of an index is usually required to indicate the overall magnitude of the effects of the UV-B radiation. The indices are almost always obtained by an integration of the downwelling UV-B total horizontal irradiances, spectrally weighted by the BSWF. Because the UV-B irradiances are measured in discrete spectral regions, some means of interpolating the irradiances at wavelengths appropriate for performing the integrations is required. The estimates of the downwelling UV-B irradiances at each nanometer are currently made using curve fitting techniques, and have come to be known as “synthetic spectra.” The synthetic spectra algorithm provides a functional form which may be used to approximate the spectral, downwelling UV-B irradiances at any wavelength within the wavelength range of the measurements. The current synthetic spectra algorithm, described in

Min and Harrison (1998) with updates by Davis and Slusser (2005), begins with a form of Beer's Law:

$$I_\lambda = I_{0,\lambda} \exp\left\{-\left(mX(\lambda) + C_1\lambda^{-1} + C_2\lambda^{-2} + C_3\lambda^{-3} + C_4\lambda^{-4}\right)\right\}, \qquad (8.11)$$

where I_0 and I are the extraterrestrial and surface spectral irradiance, respectively, at a wavelength λ, m is the atmospheric path, X is the optical depth due to ozone, and the constants C_i are determined by the fitting algorithm. When considering the method to determine the coefficients C_i, one of the first considerations is if the functional form is linear in the undetermined coefficients. In this case, the form requires a non-linear approach; in particular, the non-linear least squares approach of Levenberg and Marquardt is basically used as described in Press et al. (1992). Although taking the natural logarithm of the equation puts it in a form amenable to a linear fitting technique, it has been found through extensive testing at UVMRP, using many different functional representations of the term within the exponential, that the original non-linear form results in superior performance, particularly at the shorter wavelengths where much of the interest lies for agricultural research. Figure 8.8 shows an example of a synthetic spectrum obtained from combined UV and visible MFRSR measurements, and two important BSWFs: (1) the photosynthetically active region (PAR), and (2) the Flint BSWF region.

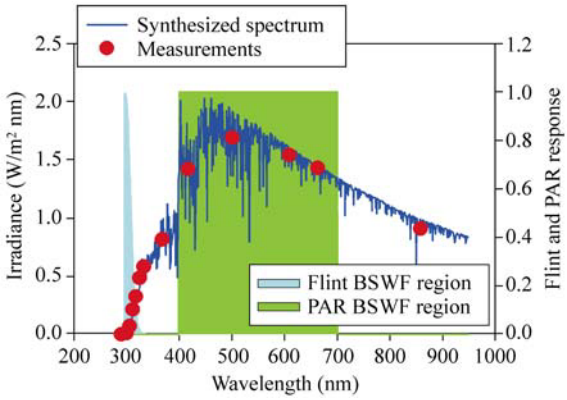

Figure 8.8 An example of a synthetic spectrum, along with the measurements from which it was derived, and the Flint and PAR BSWF regions over which the synthetic spectrum is integrated to produce agriculturally important indices. See Caldwell et al. (1986) for a discussion of the Flint BSWF

The synthetic spectrum has been applied to the data collected by UV-MFRSR instruments deployed at all US UVMRP climatological sites since 2000 to construct a database of daily sums of unweighted UV-A, unweighted UV-B, erythemal, vitamin D, and Flint and Caldwell indices. Figure 8.9 shows the annual average of the daily sum of unweighted UV-A irradiance for 2001 which was derived from

the database. The UVMRP website allows access to the daily sum database to the extent that the user is allowed to find averages of the daily sums over a user specified interval for any of the U.S. UVMRP sites.

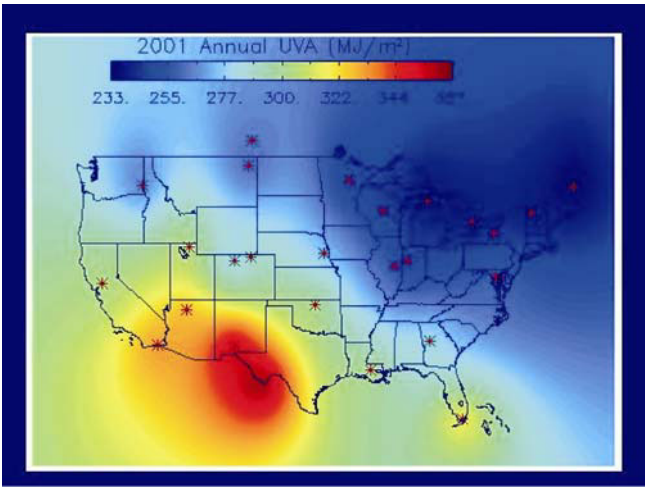

Figure 8.9 Contour map of 2001 annual accumulation of unweighted UV-A irradiance over the continental U.S. in MJ/m^2. The UVMRP station locations are identified by the red asterisks in the figure

8.6 Database Design and Website Interface

The primary objective of the UVMRP database and web design is to provide a user-friendly interface for an end user to search, view, and download data and related descriptions via the Internet. The interface was designed with the client/server paradigm. To prevent loss of data, backups are made with the use of tape, CD, and DVD, some of which are stored off site. The database containing the aforementioned measurements and derived data is implemented using the open source MySQL (DuBois, 2005). Structure Query Language (SQL) and open source Java Server Faces (JSF) are exploited to integrate different parts into this web accessible database. The database is updated daily when new measurements are collected. In this section, we briefly introduce the information that can be viewed and downloaded from the website, the database structure, and the website interface.

8.6.1 The Data

The information contained in the database can be classified into three categories: metadata, measurements, and derived data. As described in Table 8.4, metadata

include site information, instrument history at each site, calibration for each instrument/sensor, and documentation. Raw voltage measurements and calibrated data are recognized as measurements. Derived data are comprised of optical depths, column ozone, and synthetic spectra.

Table 8.4 The structure of the UV-B Database

Data in the UVMRP Database	
Meta Data	Description
Location information	Contains the geography of a location as well as internal location ID and phone number, if a phone line site
Tracking information	Contains the history of a particular instrument. Some instruments are rotated annually through the calibration facility and moved to a different location. A history of this information is maintained for special use
Calibration and angular correction data	All the calibration and angular correction data are stored in a table accessible by calibration date. The calibration factors are interpolated between starting and closing calibration data
Documentation	The quality control flags, historical instrument configurations, web interface error codes, meteorological events at locations, and users of the data are stored in a table to allow dynamic access and change to its structure
Measurements	Description
Raw voltage	Contains raw voltage measurements and quality control codes
Cosine corrected data	Contains cosine corrected data for UV-MFRSR and VIS-MFRSR instruments along with quality control codes
Calibrated data	Data used to calculate both lamp and Langley calibration are stored in tables but the actual calculation is done at the time of the data request
Derived Products	Description
Instantaneous optical depths	Time resolution of 3-min
Average optical depths	Morning and afternoon data
Column ozone	Contains daily column ozone
Synthetic Spectra	Data used to calculate synthetic spectra are stored in tables, but the actual calculation is performed at the time of the data request

To access the link for the data and derived data, go to the UVMRP website (http://uvb.nrel.colostate.edu/UVB). Click on the "Data Access" link at the top of the page where you will access the page shown in Fig. 8.10. On this page, the user can view or download the data desired by clicking on the corresponding self explanatory buttons located in the right hand column. The left hand column contains short descriptions about data from each category. Details regarding data processing and corrections are accessible through the links located at the bottom of the right hand column under "Quality Control."

Figure 8.10 Web interface of USDA UV-B Monitoring and Research Program database

8.7 UVMRP's Role in UV-B Agricultural Effects Studies

The previous sections describe UVMRP's monitoring activities and are limited to the physical aspects of UV radiation. In addition, UVMRP has played a role in the investigation of the biological response or "effects studies" of various plants and animals to UV-B and visible radiation. The goal of these studies is to evaluate the response of plants, forests, ecosystems, and animals to UV-B radiation and other climate stress factors. The program works with agricultural/forest researchers to evaluate the isolated effects of elevated UV-B on agricultural crops, livestock, forests, and range resources. Furthermore, it assesses the combined effects of UV-B radiation and other climate stress factors, such as moisture (drought), temperature, ozone, soil nutrients and CO_2. By understanding both compounding and antagonistic effects of multiple stress factors, the research will help develop solutions that

allow producers to cope with these detrimental effects and ensure quality and productivity for agriculture and livestock into the future. These studies provide a link between the knowledge of the climatology of UV-B radiation and the modeling of crop growth. The effects research is being conducted at a number of universities, and were directed and funded by UVMRP. Excerpts from this research are presented below:

At Colorado State University, Dr. Wei Gao, Dr. Heidi Steltzer, and Dr. Mathew Wallenstein evaluated the counteracting effects of UV-B radiation on litter decomposition. The study was conducted in a controlled greenhouse facility managed by Dr. Jack Morgan, USDA ARS, using aspen litter to determine if the effects of UV-B radiation on litter decomposition vary in relation to water availability and in response to suppressed biotic activity. The UVMRP designed and fabricated the UV-B lighting, control, and measurement hardware used in the study. Another CSU research scientist, Dr. Daniel Milchunas, conducted a three year study to evaluate the influence of UV-B on cattle rangeland grass decomposition and carbon storage. The UVMRP supplied UV-B monitoring instruments as well as data collection and processing services for this outdoor exclosure study.

Other examples of effects research are briefly described below, in no particular order. This list, however, is not meant to be exhaustive of all efforts associated with UVMRP. The work is separated according to the institution of the principal investigator of the study. For a more complete description of this work, the reader is directed to the citations given or to the UVMRP website.

8.7.1 Mississippi State University

Dr. K. Raja Reddy directs a group of researchers concerned with several phenomenological, growth, and physiological parameters influenced by UV-B radiation and other environmental factors. Studies of how UV-B and heat affect plants have been conducted so that cultivars better suited to high-temperature and high UV-B environments can be produced by breeders. Quantitative data on various growth and developmental processes were measured, and algorithms were developed for those processes. Ultraviolet radiation effect modules of crop growth under climate stress scenarios, such as higher temperatures and elevated CO_2 concentrations, have also been produced to incorporate the effects into models assessing the impact of climate change to assist producers and policy decision managers.

8.7.2 Purdue University

At Purdue University, Dr. Richard Grant and his colleagues conducted a number of empirical, field canopy, and greenhouse studies to determine the effects of

UV-B on various plants. Their work included determination of the response of soybean and sorghum to enhanced UV-B, and also its effect on biomass and its distribution. Particular emphasis was placed on the reaction of plant leaf physiology to the UV-B radiation. The group also studied the penetration of UV-B in oak-hickory forest, in a mature maize canopy and into the understory of a leafing-out deciduous forest. Model studies were performed on vegetation exposure, including that of Asian Soybean Rust, for a 3-day trajectory of an actual event in Iowa in September 2007.

8.7.3 Utah State University

Dr. Ron Ryel, Mr. Stephen Flint, and colleagues from Utah State University, combined numerous UV radiation related studies to determine and evaluate various UV-B and UV-A biological weighting functions. Weighted UV doses based on this and other work are routinely calculated and posted on the UVMRP website. Field experiments were conducted on Mauna Kea, HI at approximately 3000 m elevation to test the relative importance of the UV-B and UV-A wavebands under near ambient, no UV-B, and no UV-A or UV-B conditions.

8.7.4 University of Maryland

Dr. Joseph Sullivan (University of Maryland) and Dr. Stephen Britz (USDA Food Components and Health Lab, Beltsville, MD) conducted numerous field, greenhouse and growth chamber studies over the past eight years to determine responses of plants to UV-B radiation. A primary goal of their research was to understand the dose response (e.g., total energy absorbed) and wavelength response (e.g., impact of specific components of the solar spectrum) of plants in terms of damage, and the induction of protective mechanisms by sunlight. These studies, which are focused on important agricultural (e.g., soybean and barley) and forest (e.g., loblolly pine and hybrid poplar) species, utilized the high resolution UV data provided by UVMRP.

8.7.5 Washington State University

Dr. John Bassman and his colleagues conducted studies focused on the effects of enhanced UV-B on secondary chemistry in forage species, and the consequences for nutrition of specialist and generalist mammalian herbivores. The objectives of the studies were to: (1) determine the effects of enhanced solar UV-B radiation on

the concentration of key classes of secondary compounds from both the shikimate acid and mevalonic acid pathways in forage species with inherently different levels of these compounds; (2) identify selected key compounds of potential importance to herbivore nutrition where changes were significant; (3) quantify effects of enhanced UV-B on nutritional quality of these same forage species for a specialist and generalist mammalian herbivore through preference, intake and digestibility; and (4) relate changes in secondary plant chemistry to nutritional responses.

8.7.6 University of Illinois — Chicago

Dr. Katherine Warpeha and Dr. Lon Kaufman used a UVMRP UV-B light source in experiments designed to study the effects of UV-A and UV-B radiation on early development of soybean. The goals of the study were to: (1) quantify the effects of UV radiation on the early development of soybean and to help define ways to evaluate the effects of UV radiation; (2) evaluate the effects of UV radiation on the products of the phenylpropanoid pathway; and (3) initiate experiments to test stable transformation of young soybean seedlings with full length Prephenate Dehydratase1 (PD1) in order to determine if additional PD1 expression confers increased protection from UV radiation.

8.7.7 Highlights of Other Collaborations

In addition to the UVMRP sponsored and funded research efforts described in Sections 8.7.1 through 8.7.6, further research collaborations include:

Cornell University: Dr. Craig N. Austin has focused his research on how UV-B radiation affects the development of powdery mildew on the fruit and foliage of wine grape plants grown in the Finger Lakes Region of New York State. For two summers, the UVMRP supplied a portable UV-B monitoring instrument used in some components of the studies. The objectives of these studies were to: (1) determine the effects of shading versus direct sun exposure on the development of powdery mildew on both fruit and foliage, and investigate the possible mechanisms involved; (2) determine the degree of powdery mildew control provided by exposing fruit and foliage to sunlight via practices such as pruning, training, and leaf pulling; and (3) investigate the interaction of sun exposure and plant water status on powdery mildew development.

USDA Animal and Plant Health Inspection Service: For three consecutive winters from 2001 to 2004, the UVMRP supplied two UV monitoring stations to the USDA APHIS, Veterinary Services, National Animal Health Programs Wildlife Disease group to study the effect of UV radiation on brucellosis persistence in the

Yellowstone National Park ecosystem. The research on the transmission of this potentially devastating disease is a major priority which has involved federal and state agencies, animal health professionals, wildlife professionals and enthusiasts, and cattle ranchers in Montana and Wyoming. Preliminary findings from the study suggest that UV radiation plays a large role in the degradation of Brucella abortus. This finding suggests that continued monitoring of UV radiation levels could be an important tool in managing the disease.

Southern University: Responses of 35 tree species to UV-B radiation are being quantified by Dr. Yadong Qi.

University of California, Davis, Desert Research and Extension Service: Dr. Paul Sebesta is investigating the effect of UV-B and PAR in comparing sugarcane yields for ethanol production in Southern California, Louisiana, and Florida.

University of Nebraska at Lincoln: Dr. Elizabeth Walter-Shea and Dr. Kenneth Hubbard conducted investigations of UV radiation levels within vegetative canopies, and how these levels affect microoganisms.

8.8 Modeling of Agricultural Sustainability

In addition to the monitoring and the effects studies of UV radiation, the UVMRP conducts research on crop growth and production assessment modeling. The goal of the modeling work is to couple a regional climate forecasting model, such as the Climate version-Weather Research and Forecasting Model (CWRF), to crop growth models to assess the role of global climate change on future crop health and crop yields. The main thrust of this effort is to develop an Integrated Agricultural Impact Assessment System (IAIAS) in collaboration with a group at the University of Illinois, Urbana-Champaign, led by Dr. Xin-Zhong Liang. The goal of IAIAS is to develop an integrated system that fully couples the earth's climate, UV-visible solar radiation, and crop growth models, and assimilates satellite and in-situ observations to ultimately predict climate-crop interactions. This effort will facilitate model sensitivity studies thus providing credible information on crop responses to regional climate variability and changes for decision makers to determine optimal cultural practices, assess potential risks, and identify risk management strategies. The coupled model results can be directly validated with the UVMRP UV and PAR measurements, while offering a unique tool to predict crop life cycle processes over the entire U.S. The initial results of the coupled GOSSYM (a cotton growth model) and CWRF models are shown in Fig. 8.11, which displays modeled cotton yields that agree to within ±15% of actual yields at most sites for the 27 years of data accumulated over the entire 14-state region of the Cotton Belt.

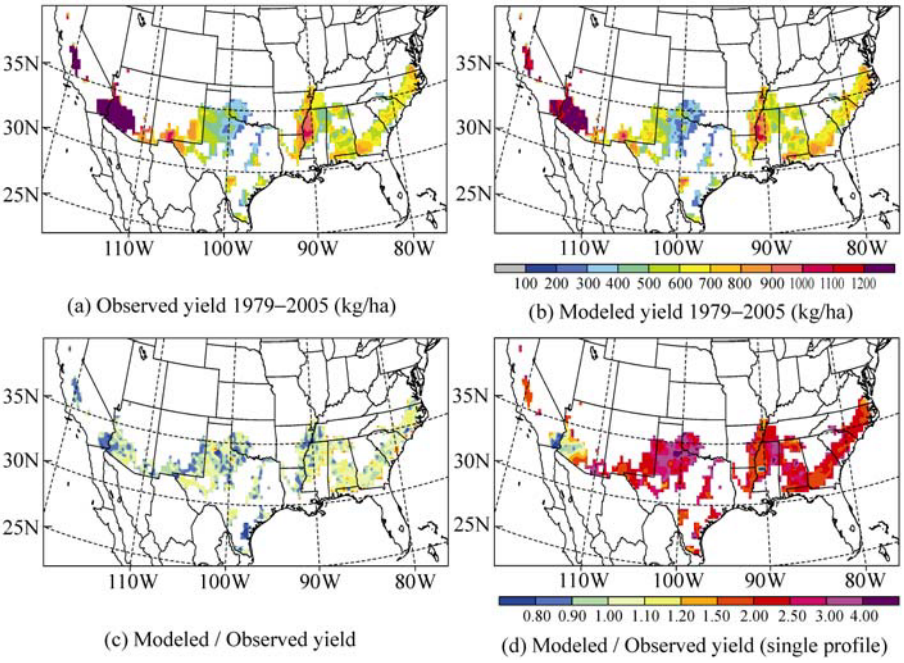

Figure 8.11 Comparison of the long-term observed average of cotton yield in the 14-state Cotton Belt region and that predicted by the coupled GOSSYM-CWRF model. Geographic distributions of the 1979 – 2005 mean cotton yields (kg ha^{-1}): (a) observed and (b) simulated by the new GOSSYM; and of the ratios for the mean cotton yields over observations as simulated by (c) the new and (d) original GOSSYM

8.9 Future Considerations

The USDA UVMRP is constantly reviewing its research goals and evaluating the needs expressed by the stakeholders in USDA research. Although fiscal years 2007, 2008 and 2009 saw budget reductions, the activities at UVMRP are ongoing in a manner as to consistently respond to the needs of the agricultural research community in the best possible manner.

With an eye toward the future, UVMRP also collaborates with developers of UV products from satellite observations. While satellite platforms have a more restrictive temporal sampling program, they offer superior geographic coverage. One challenge to the satellite community is that retrieval of surface UV irradiance requires correction for presence of clouds and aerosols. As an example of how well satellite data can be used at a particular site, data from NASA's CERES SYNI (Clouds and the earth's Radiant Energy System, SYNoptic Interpolated) program is shown in Fig. 8.12. The retrieved UV-A irradiances compare with UV-A irradiance derived from the UVMRP synthetic spectrum to within 0.6 watts/m^2 in the mean with an RMS difference of 5.6 watts/m^2 for this particular case.

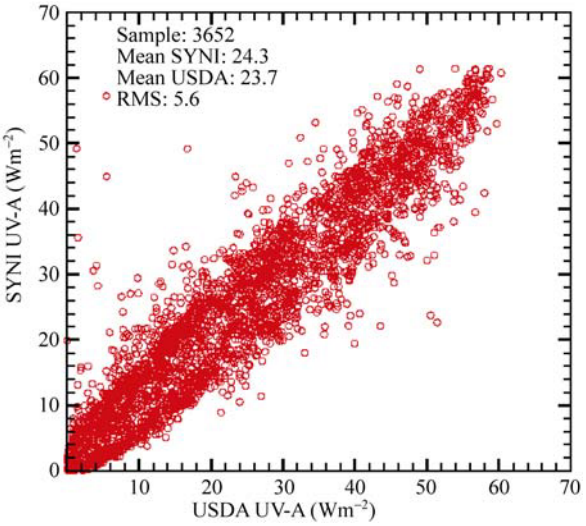

Figure 8.12 Satellite retrieved values of unweighted UV-A total horizontal irradiance compared to the same quantities deduced from a synthetic spectrum fit to UV-MFRSR data measured at the DOE Atmospheric Radiation Monitoring Program's Southern Great Plains site near Ponca City, OK during July 2002 (satellite retrieved data provided by NASA CERES SYNI effort)

Conversely, as an example of the spatial coverage provided by the USDA UVMRP network, the UV Index from the Total Ozone Mapping Spectrometer (TOMS) is compared to gridded values from the UVMRP values (Gao et al., 2009) averaged over the summers from 2000 through 2004. Figure 8.13 shows two examples that demonstrate the level of agreement between the surface and satellite monitoring communities, and lends hope that resources may be focused between the two efforts in obtaining higher quality products useful to agricultural, medical, industrial and meteorological researchers.

8.10 Summary

This chapter has described the data and products of the USDA UVMRP. These datasets are available to the public and can be accessed via the Internet. The monitoring network consists of 37 observation sites covering the continental U.S., along with coverage of Alaska and Hawaii, southern Canada, and southern New Zealand. Multifilter Shadowband Rotating radiometers are deployed to make spectral irradiance measurements in the UV and visible wavelength regions. The erythemally weighted UV radiation is measured by broadband pyranometers. The PAR is also measured for use in agricultural research. The program has been providing quality UV-B radiation data to researchers throughout the agricultural, medical, industrial, and atmospheric research communities since 1993. The primary

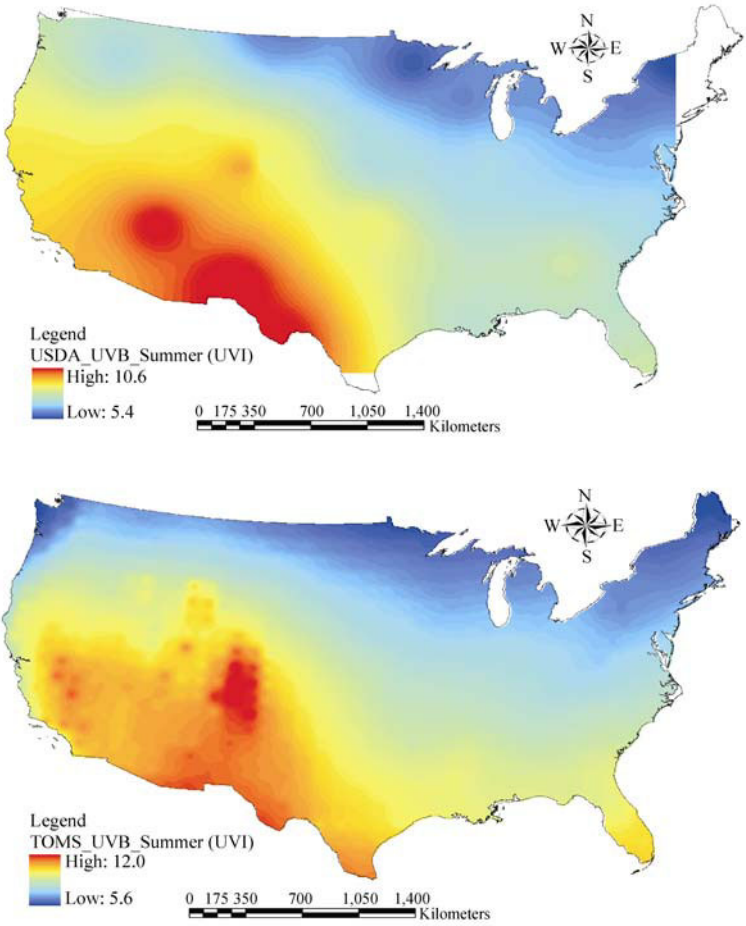

Figure 8.13 Comparison of the UV index from USDA UVMRP (top) averaged over the summers of 2000 – 2004 and the same quantity from NASA TOMS (bottom) as reported in Gao et al. (2009). The UVMRP UV indices span from 5.4 to 9.0 while the TOMS values range from 5.6 to 12.0

raw voltage measurements are available by special request. With our research in instrumentation, correction techniques, system stability, and statistical analysis, high quality calibrated data have been produced as second level products. These data furnish researchers in agriculture, ecology, environment, meteorology, human health, and related specialties with valuable information not available elsewhere. Based on our research results, optical depths, daily column ozone, and synthetic spectra are derived using spectral UV-B measurements, plus spectral irradiances in the visible region. The USDA UVMRP receives numerous requests for its products from researchers in agriculture, atmospheric monitoring, human and animal health, and industrial product quality concerns. The UVMRP is collaborating with the broader scientific community, with an eye toward the future, to focus its activities

and resources to best serve the needs of researchers across a wide spectrum of scientific and social activities.

Acknowledgements

The USDA UVMRP was sponsored during 2007 – 2008 by USDA CSREES under Hatch/Multistate, Contract Number: COL-00-250-W502 and during 2006 – 2007 by USDA CSREES under Contract Number: 2006-34263-16926. The UVMRP effort would not have been possible without the contributions of its staff: Ms. Becky Olson, Mr. Scott Janssen, Mr. Bill Durham and Ms. Rita Deike. A special appreciation is extended to Mr. George Janson for final editing and compilation of figures and to Dr. Xinli Wang for his assistance in the initial drafts of this chapter.

References

Barkstrom BR (1984) The Earth Radiation Budget Experiment (ERBE). Bull. Amer. Meteor. Soc. 65:1170 – 1185

Bassman JH (2004) Ecosystem consequences of enhanced solar ultraviolet radiation: secondary plant metabolites as mediators of multiple trophic interactions in terrestrial plant communities. Photochemistry and Photobiology 79(5): 382 – 398

Bigelow DS, Slusser JR, Beaubien AF, and Gibson JH (1998) The USDA Ultraviolet Radiation Monitoring Program. Bulletin of the American Meteorological Society 79(4): 601 – 615

Bigelow DS, and Slusser JR (2000) Establishing the stability of multifilter UV rotating shadow-band radiometers. Journal of Geophysical Research 105(D4): 4833 – 4840

Blumthaler M, and Ambach W (1990) Indication of increasing solar ultraviolet-B radiation flux in Alpine regions. Science 248(4952): 206 – 208

Bodhaine BA, Dutton EG, McKenzie RL, and Johnston PV (1998) Calibrating broadband UV instruments: ozone and solar zenith angle dependence. Journal of Atmospheric and Oceanic Technology 15(4): 916 – 926

Bodhaine BA, Wood NB, Dutton EG, and Slusser JR (1999) On Rayleigh optical depth calculations. Journal of Atmospheric and Oceanic Technology 16: 1854 – 1861

Bredahl L, Ro-Poulsen H, and Mikkelsen TN (2004) Reduction of the ambient UV-B radiation in the high-arctic increases F_v/F_m in *salix arctica* and *vaccinium uliginosum* and reduces stomatal conductance and internal CO_2 concentration in *salix arctica*. Arctic, Antarctic, and Alpine Research 36(3): 364 – 369

Bucholtz A (1995) Rayleigh-scattering calculations for the terrestrial atmosphere. Applied Optics 34(15): 2765 – 2773

Caldwell MM, Camp CW, Warner CW, and Flint SD (1986) Action spectra and their role in assessing biological consequences of solar UV-B radiation change. In: Worrest RC, Caldwell MM (eds) Stratospheric Ozone Reduction, Solar Ultraviolet Radiation and Plant Life. Springer-Verlag, pp.87 – 111

Caldwell MM, Ballaré CL, Bornman JF, Flint SD, Björn LO, Teramura AH, Kulandaivelu G, and Tevini M (2003) Terrestrial ecosystems, increased solar ultraviolet radiation and interactions with other climatic change factors. Photochemical and Photobiological Sciences 2(1): 29 – 38

Clarke A, and Harris CM (2003) Polar marine ecosystems: major threats and future change. Environmental Conservation 30(1): 1 – 25

Davis JM, and Slusser J (2005) New USDA UVB synthetic spectra algorithm. In: Bernhard G, Slusser JR, Herman JR, Gao W (eds) Ultraviolet Ground- and Space-Based Measurements, Models, and Effects V. Proceedings of SPIE Vol. 5886 (SPIE, Bellingham, WA, 2005), pp. 58860B-1-58860B-7

Disterhoft P (2005) Stability characteristics of 1000 watt FEL-type QTH lamps during the seasoning and screening process. In: Bernhard G, Slusser JR, Herman JR, Gao W (eds) Ultraviolet Ground- and Space-based Measurements, Models, and Effects V, Proceedings of SPIE Vol 5886, SPIE, 58860G

DuBois Paul (2005) MySQL™ The definitive guide to using, programming, and administering MySQL 4.1 and 5.0, Third Edition. Sams Publishing, Indianapolis, IN, USA

Early E, Thompson A, Johnson C, DeLuisi J, Disterhoft P, Wardle D, Wu E, Mou W, Sun Y, Lucas T, Mestechkina T, Harrison L, Berndt J, and Hayes DS (1998a) The 1995 North American interagency intercomparison of ultraviolet monitoring spectroradiometers. Journal of Research of the National Institute of Standards and Technology 103(1): 15 – 62

Early E, Thompson A, Johnson C, DeLuisi J, Disterhoft P, Wardle D, Wu E, Mou W, Ehramjian J, Tusson J, Mestechkina, Beaubian M, Gibson J, and Hayes D (1998b) The 1996 North American interagency intercomparison of ultraviolet monitoring spectroradiometers. Journal of Research of the National Institute of Standards and Technology 103(5): 449 – 482

Farman JC, Gardiner BG, and Shanklin JD (1985) Large losses of total ozone in Antarctica reveal seasonal ClO_x/NO_x interaction. Nature 315: 207 – 210

Flint SD, Ryel RJ, and Caldwell MM (2003) Ecosystem UV-B experiments in terrestrial communities: a review of recent findings and methodologies. Agricultural and Forest Meteorology 120: 177 – 189

Frederick JE, and Snell HE (1988) Ultraviolet radiation levels during the Antarctic spring. Science 241(4864): 438 – 440

Fröhlich C, and Shaw GE (1980) New determination of Rayleigh scattering in the terrestrial atmosphere. Applied Optics 19(11): 1773 – 1775

Gao W, Slusser J, Gibson J, Scott G, Bigelow D, Kerr J, and McArthur B (2001) Direct-Sun column ozone retrieval by the ultraviolet multifilter rotating shadow-band radiometer and comparison with those from Brewer and Dobson spectrophotometers. Applied Optics, 40(19): 3149 – 3155

Gao W, Grant RH, Heisler GM, and Slusser JR (2002) A geometric ultraviolet-B radiation transfer model applied to vegetation canopies. Agronomy Journal 94: 475 – 482

Gao W, Grant RH, Heisler GM, and Slusser JR (2003) UV-B radiation in a row-crop canopy: An extended 1-D model. J. Agric. Forest Meteorol. 120: 141 – 151

Gao W, Gao ZQ, and Chang NB (2009) Comparative analysis of UVB exposure between Nimbus 7/TOMS satellite estimates and ground-based measurements. In: Gao W, Schmoldt D,

Slusser JR (eds) UV Radiation in Global Change: Measurements, Modeling and Effects on Ecosystems. Springer-Verlag and Tsinghua Univ. Press

Gibson JH (ed) (1991) Justification and criteria for the monitoring of ultraviolet (UV) radiation: Report of UV-B measurements workshop (URL: http://uvb.nrel.colostate.edu/UVB/publications/91_workshop.pdf)

Gibson JH (1992) Criteria for status-and-trends monitoring of ultraviolet (UV) radiation: Recommendations of the UV-B Monitoring Workshop (URL: http://uvb.nrel.colostate.edu/UVB/publications/92_report.pdf)

Grainger RG, Basher RE, and McKenzie RL (1993) UV-B Robertson-Berger meter characterization and field calibration. Applied Optics 32(3): 343 – 349

Grant RH (1999) Potential effect of soybean heliotropism on ultraviolet-B irradiance and dose. Agronomy Journal 91: 1017 – 1023

Grant WB (1988) Global stratospheric ozone and UVB radiation. Science 242(4882): 1111

Gröbner J, Blumthaler M, and Ambach W (1996) Experimental investigation of spectral global irradiance measurement errors due to a non ideal cosine response. Geophysical Research Letters 23(18): 2493 – 2496

Hand JL, Kreidenweis SM, Slusser J, and Scott G (2004) Comparisons of aerosol optical properties derived from Sun photometry to estimates inferred from surface measurements in Big Bend National Park, Texas. Atmospheric Environment 38: 6813 – 6821

Harrison L, and Michalsky J (1994) Objective algorithms for the retrieval of optical depths from ground-based measurements. Applied Optics 33(22): 5126 – 5132

Harrison L, Michalsky J, and Berndt J (1994) Automated multifilter rotating shadow-band radiometer: an instrument for optical depth and radiation measurements. Applied Optics 33(22): 5118 – 5125

Herman JR, Bhartia PK, Ziemke J, Ahmad Z, and Larko D (1996) UV-B increases (1979 – 1992) from decreases in total ozone. Geophysical Research Letters 23(16): 2117 – 2120

Janson GT, Slusser JR, Scott G, Disterhoft P, and Lantz K (2004) Long-term stability of UV multifilter rotating shadowband radiometers, part 2: lamp calibrations versus the Langley method. In: Slusser JR, Herman JR, Gao W, Bernhard G (eds) Ultraviolet Ground- and Space-based Measurements, Models, and Effects IV. Proceedings of SPIE Vol 5545, SPIE, 43 – 48

Jaque F, Tocho JO, DaSilva LF, Bertuccelli G, Crino E, Cusso F, DeLaurentis MA, Hormaechea JL, Lifante G, Nicora MG, Ranea-Sandoval HF, Valderrama V, and Zoja GD (1994) Ground-based ultraviolet radiation measurements during springtime in the southern hemisphere. Europhysics Letters, 28(4): 289 – 293

Kakani VG, Reddy KR, Zhao D, and Sailaja K (2003) Field crop responses to ultraviolet-B radiation: a review. Agricultural and Forest Meteorology 120: 191 – 218

Kerr JB (2005) Understanding the factors that affect surface ultraviolet radiation. Optical Engineering, 44(4): 041002-1 – 041002-9

Kerr JB, and McElroy CT (1993) Evidence for large upward trends of ultraviolet-B radiation linked to ozone depletion. Science 262(5136): 1032 – 1034

Kulandaivelu G, and Tevini M (2003) Terrestrial ecosystems, increased solar ultraviolet radiation and interactions with other climatic change factors. Photochemical and Photobiological Sciences 2(1): 29 – 38

Landelius T, and Josefsson W (2000) Methods for cosine correction of broadband UV data and their effect on the relation between UV irradiance and cloudiness. Journal of Geophysical Research 105(D4): 4785 – 4802

Lantz KO, Disterhoft P, DeLuisi JJ, Early E, Thompson A, Bigelow D, and Slusser J (1999) Methodology for deriving clear-sky erythemal calibration factors for UV broadband radiometers of the U.S. Central UV Calibration Facility. Journal of Atmospheric and Oceanic Technology 16: 1736 – 1752

Lantz K, Disterhoft P, Early E, Thompson A, DeLuisi J, Berndt J, Harrison L, Kiedron P, Ehramjian J, Bernhard G, Cabasug L, Robertson J, Mou W, Taylor T, Slusser J, Bigelow D, Durham B, Janson G, Hayes D, Beaubien M, and Beaubien A (2002) The 1997 North American interagency intercomparison of ultraviolet spectroradiometers including narrowband filter radiometers. Journal of Research of the National Institute of Standards and Technology 107(1): 19 – 62

Lantz K, Disterhoft P, Wilson C, Janson G, Slusser J, Bloms S, and Michalsky J (2005) Out-of-band rejection studies of the UV Multi-Filter Rotating Shadow-band radiometers. In: Schäfer K, Comerón A, Slusser JR, Picard RH, Carleer MR, Sifakis N (eds) Remote Sensing of Clouds and the Atmosphere X, Proceedings of SPIE Vol 5979, SPIE, 59791N

Lean J (1991) Variations in the Sun's radiative output. Reviews of Geophysics 29: 505 – 535

Lean JL, Rottman GJ, Kyle HL, Woods TN, Hickey JR, and Puga LC (1997) Detection and parameterization of variations in solar mid- and near-ultraviolet radiation (200 nm – 400 nm). Journal of Geophysical Research 102 (D25): 29939 – 29956

Leszczynski K, Jokela K, Ylianttila L, Visuri R, and Blumthaler M (1998) Erythemally weighted radiometers in solar UV monitoring: results from the WMO/STUK intercomparison. Photochemistry and Photobiology, 67(2): 212 – 221

Li Y, Yue M, and Wang XL (1998) Effects of enhanced ultraviolet-B radiation on crop structure, growth and yield components of spring wheat under field conditions. Field Crops Research 57(3): 253 – 263

LI-COR, Inc. (1991) LI-COR Terrestrial Radiation Sensors, Type SA Instruction Manual. LI-COR, Lincoln, NE, USA

Marggraf WA, and Griggs M (1969) Aircraft measurements and calculations of the total downward flux of solar radiation as a function of altitude. Journal of the Atmospheric Sciences 26: 469 – 476

Mayer B, and Seckmeyer G (1996) All-weather comparison between spectral and broadband (Robertson-Berger) UV measurements. Photochemistry and Photobiology 64(5): 792 – 799

McKenzie R, Bodeker G, Scott G, Slusser J, and Lantz K (2006) Geographical differences in erythemally-weighted UV measured at mid-latitude USDA sites. Photochemical and Photobiological Sciences (5): 343 – 352

McKenzie RL, Aucamp PJ, Bais AF, Björn LO, and Ilyas M (2007) Changes in biologically-active ultraviolet radiation reaching the Earth's surface. Photochemical and Photobiological Sciences 6(3): 218 – 231

McKinlay AF, and Diffey BL (1987) A reference action spectrum for ultraviolet induced erythema in human skin. CIE-Journal 6(1): 17 – 22

Michalsky JJ, Perez R, Stewart R, LeBaron BA, and Larrison L (1988) Design and development of a rotating shadowband radiometer solar radiation/daylight network. Solar Energy 41(6): 577 – 581

Michalsky JJ, Harrison LC, and Berkheiser WE III (1995) Cosine response characteristics of some radiometric and photometric sensors. Solar Energy 54(6): 397 – 402

Min Q, and Harrison LC (1998) Synthetic spectra for terrestrial ultraviolet from discrete measurements. Journal of Geophysical Research 103(D14): 17033 – 17039

Newchurch MJ, Yang E-S, Cunnold DM, Reinsel GC, Zawodny JM, and Russell JM III (2003) Evidence for slowdown in stratospheric ozone loss: First stage of ozone recovery. Journal of Geophysical Research 108(D16): 4507, DOI:10.1029/2003JD003471

O'Hara F, and O'Hara L (eds) (1993) Report. UV-B Critical Issue Workshop, Cocoa Beach, FL, Center for Global and Environmental Studies, Oak Ridge National Laboratory

Press WH, Teukolsky SA, Vetterling WT, and Flannery BP (1992) Numerical Recipes in C: the art of scientific computing. Second Edition, Cambridge University Press

Reddy KR, Kakani VG, Zhao D, Mohammed AR, and Gao W (2003) Cotton responses to ultraviolet-B radiation: experimentation and algorithm development. Agricultural and Forest Meteorology 120: 249 – 265

Reinsel GC, Miller AJ, Weatherhead EC, Flynn LE, Nagatani RM, Tiao GC, and Wuebbles DJ (2005) Trend analysis of total ozone data for turnaround and dynamical contributions. Journal of Geophysical Research 110:D16306, DOI:10.1029/2004JDD004662

Rozema J, van de Staaij J, Björn LO, and Caldwell M (1997) UV-B as an environmental factor in plant life: stress and regulation. Trends in Ecology and Evolution 12(1): 22 – 28

Schmid B, and Wehrli C (1995) Comparison of Sun photometer calibration by use of the Langley technique and the standard lamp. Applied Optics 34(21): 4500 – 4512

Schmid B, Spyak PR, Biggar SF, Wehrli C, Sekler J, Ingold T, and Mämpfer N (1998) Evaluation of the applicability of solar and lamp radiometric calibrations of a precision Sun photometer operating between 300 nm and 1025 nm. Applied Optics 37(18): 3923 – 3941

Science and Policy Associates (1992) Report. UV-B Monitoring Workshop: A review of the science and status of measuring and monitoring programs, Washington, DC, Science and Policy Associates, Inc

Scotto J, Cotton G, Urbach F, Berger D, and Fears T (1988) Biologically effective ultraviolet radiation: surface measurements in the United States, 1974 to 1985. Science 239(4841): 762 – 764

Seckmeyer G, Bais AF, Bernhard G, Blumthaler M, Booth CR, Lantz RL, McKenzie RL, Disterhoft P, and Webb A (2007) Instruments to measure solar ultraviolet radiation. Part 2: Broadband instruments measuring erythemally weighted solar irradiance. WMO/GAW No. 164, World Meteorological Organization, Geneva

Shaw GE (1982) Solar spectral irradiance and atmospheric transmission at Mauna Loa Observatory. Applied Optics 21(11): 2006 – 2011

Shettle EP, and Anderson SM (1995) New visible and near IR ozone absorption cross-sections from MODTRAN. In: Anderson GP, Picard RH, Chetwynd JH (eds) Proceedings of the 17th Annual Review Conference on Atmospheric Transmission Models, Phillips Laboratory, Directorate of Geophyiscs, Hanscom Air Force Base, MA, pp. 335 – 345

Slusser J, Gibson J, Bigelow D, Kolinski D, Disterhoft P, Lantz K, and Beaubien A (2000) Langley method of calibrating UV filter radiometers. Journal of Geophysical Research 105(D4): 4841 – 4849

Smith RC, Préselin BB, Baker KS, Bidigare RR, Boucher NP, Coley T, Karentz D, MacIntyre S, Matlick HA, Menzies D, Ondrusek M, Wan Z, and Waters KJ (1992) Ozone depletion: ultraviolet radiation and phytoplankton biology in Antarctic Waters. Science 255(5047): 952 – 959

Staehelin J, Harris NRP, Appenzeller C, and Eberhard J (2001) Ozone trends: A review. Reviews of Geophysics 39(2): 231 – 290

Stephens GL (1994) Remote Sensing of the Lower Atmosphere: An Introduction. Oxford University Press, New York, p. 253

Stolarski R, Bojkov R, Bishop L, Zerefos C, Staehelin J, and Zawodny J (1992) Measured trends in stratospheric ozone. Science, 256(5055): 342 – 349

Tegelberg R, Aphalo PJ, and Julkunen-Tiitto R (2002) Effects of long-term, elevated ultraviolet-B radiation on phytochemicals in the bark of silver birch (*Betula pendula*). Tree Physiology 22: 1257 – 1263

Teillet PM (1990) Rayleigh optical depth comparisons from various sources. Applied Optics 29(13): 1897 – 1900

Teramura AH, Sullivan JH, and Ziska LH (1990) Interaction of elevated ultraviolet-B radiation and CO_2 on productivity and photosynthetic characteristics in wheat, rice, and soybean. Plant Physiology 94: 470 – 475

Thomason LW, Herman BM, and Reagan JA (1983) The effect of atmospheric attenuators with structured vertical distributions on air mass determinations and Langley plot analyses. Journal of the Atmospheric Sciences 40(7): 1851 – 1854

Turtola S, Rousi M, Pusenius J, Yamaji K, Heiska S, Tirkkonen V, Meier B, and Julkunen-Tiitto R (2005) Clone-specific responses in leaf phenolics of willows exposed to enhanced UVB radiation and drought stress. Global Change Biology 11: 1655 – 1663

Vijayaraghavan S, and Goswami DY (2002) On the calibration of a solar UV radiometer to measure broadband UV radiation from blacklight lamps. Journal of Solar Energy Engineering 124: 317 – 319

Warren JM, Bassman JH, Fellman JK, Mattinson DS, and Eigenbrode S (2003) Ultraviolet-B radiation alters phenolic salicylate and flavonoid composition of *Populus trichocarpa* leaves. Tree Physiology 23: 527 – 535

Wilson SR, and Forgan BW (1995) *In situ* calibration technique for UV spectral radiometers. Applied Optics 34(24): 5474 – 5484

WMO (World Meteorological Organization) (1989) Scientific Assessment of Stratospheric Ozone: 1989. Global Ozone Research and Monitoring Project. Vol. 1, Report No. 20, World Meteorological Organization, Geneva

WMO (2007) Scientific Assessment of Ozone Depletion: 2006. Global Ozone Research and Monitoring Project. Report No. 50, p.572, Geneva, Switzerland

Worrest RC, Smythe KD, and Tait AM (1989) Linkages between climate change and stratospheric ozone depletion. In: White JC (ed) Global Climate Change Linkages, Acid Rain, Air Quality and Stratospheric Ozone. Elsevier Science, pp.67 – 78

Xu G, and Huang X (2000) Characterization and calibration of broadband ultraviolet radiometers. Metrologia 37: 235 – 242

Xu G, and Huang X (2003) Calibration of broadband UV radiometers — methodology and uncertainty evaluation. Metrologia 40: S21 – S24

Yankee Environmental Systems, Inc. (2000) UVB-1 Ultraviolet Pyranometer Installation and User Guide, Version 2.0

Young AT (1981) On the Rayleigh-scattering optical depth of the atmosphere. Journal of Applied Meteorology 20: 328 – 330